Climate Dynamics
https://doi.org/10.1007/s00382-018-4326-9

Enhanced connections between summer precipitation over the Three-River-Source region of China and the global climate system

Bo Sun[1,2,3] · **Huijun Wang**[1,2,3]

Received: 23 November 2017 / Accepted: 26 June 2018

Abstract
This study reveals an enhanced correlation between the interannual variability of summer precipitation over the Three-River-Source (TRS) region of China and North Atlantic Oscillation (NAO), western Indian Ocean sea surface temperature (SST), El Niño-Southern Oscillation (ENSO), and the East Asian summer monsoon (EASM) for past decades, revealing an enhanced connection between the summer climate of the TRS region and the global climate system. Underlying causes are investigated based on a comparison on the climate effects associated with the aforementioned factors between periods 1961–1980 and 1991–2014. Enhanced connections to NAO are mainly attributed to the fact that the increased atmospheric moisture over the Arctic region has an enhanced latent heating on convective activity over the Hudson Bay-Davis Strait region under negative-phase NAO, generating an intensified anomalous high over Greenland and further stimulating an Eurasian wave-train influencing the TRS region. Similarly, for an El-Niño decaying summer, convection anomalies over the Maritime Continent are more significant due to enhanced latent heating observed in 1991–2014, which in turn have a more significant influence on the summer climate in TRS region. Regarding western Indian Ocean SSTs, warming in the western Indian Ocean is characterized by a warming center north (south) of the equator for 1991–2014 (1961–1980); correspondingly, the associated Kelvin wave-induced Ekman divergence mechanism is more pronounced over the Bay of Bengal and South China Sea for 1991–2014. Enhanced connections to the EASM are mainly attributable to a combined effect of Indian Ocean warming and anomalous convective activity over the Maritime Continent associated with ENSO.

Keywords Three-River-Source · Precipitation · Interannual variability · NAO · ENSO · Indian Ocean

1 Introduction

The Three-River-Source (TRS) region is where three important rivers in China originate, i.e., the Yangtze, Yellow, and Lantscang Rivers (Fig. 1). Located in central and eastern areas of Tibetan Plateau, the elevation of the TRS region mostly ranges between 3500 and 5000 m, and the surface pressure mostly ranges from 650 to 550 hPa during the summer. Southwesterlies and northwesterlies converge over the TRS region during the summer (Fig. 1), inducing a large amount of precipitation accounting for 60% of total annual precipitation occurring in the TRS region. The climate change over the TRS region is critical to water resources and to environment and ecosystems across China (Fan et al. 2010; Qian et al. 2010; Liu et al. 2014a).

Climatically, summer precipitation occurring over the TRS region is closely related to southwesterlies driven by the East Asian summer monsoon (EASM), which bring warm and moist air from the Indian Ocean to the TRS region (Li et al. 2009). Several factors have been recognized to influence the interannual variability of the EASM and of the East Asian summer climate, including El Niño-Southern Oscillation (ENSO), North Atlantic Oscillation (NAO), tropical sea surface temperatures (SSTs), and westerlies over the Tibetan Plateau (Chang et al. 2000;

✉ Bo Sun
sunb@nuist.edu.cn

[1] Key Laboratory of Meteorological Disaster, Ministry of Education, Nanjing University of Information Science and Technology, Nanjing 210044, China

[2] Collaborative Innovation Center on Forecast and Evaluation of Meteorological Disasters, Nanjing University of Information Science and Technology, Nanjing 210044, China

[3] Nansen-Zhu International Research Centre, Institute of Atmospheric Physics, Chinese Academy of Sciences, Beijing 100029, China

Published online: 27 June 2018

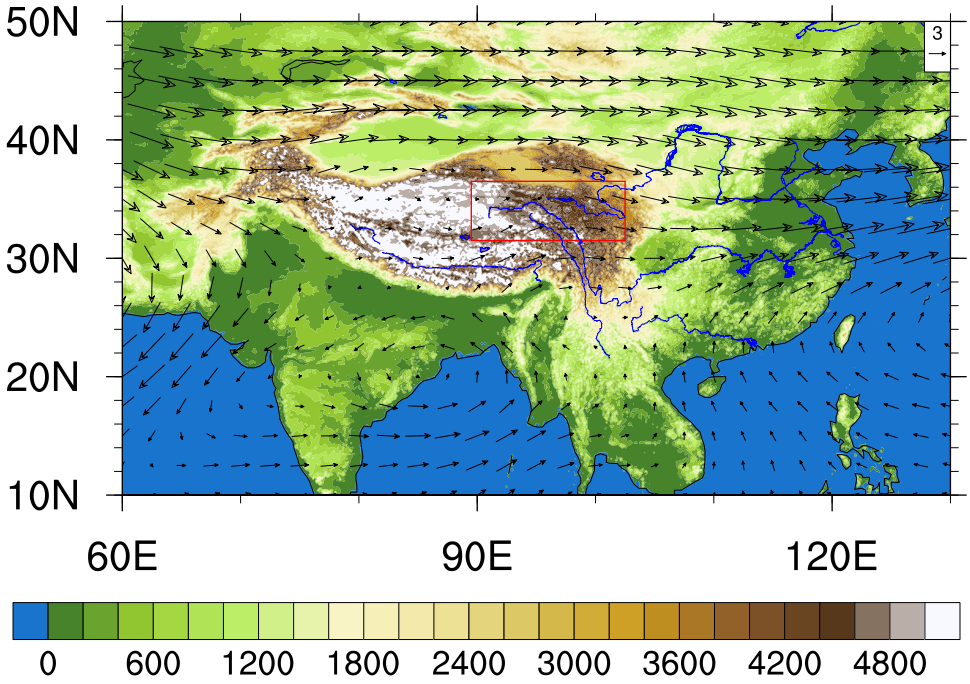

Fig. 1 Topography of the TRS region (colored shading, unit: m) and climatology of JJA 500 hPa winds for 1961–2014 (vectors, unit: m s^{-1}). Blue contours denote rivers. The red rectangle denotes the domain of the TRS region

Wang et al. 2000; Wang 2002; Wu et al. 2009; Sun and Wang 2012; Song and Zhou 2014; Chiang et al. 2017; Xue and Zhao 2017). Of these factors, NAO and ENSO are considered to be central to the interannual variability of TRS summer precipitation (Sun and Wang 2018). In focusing on 1979–2014, Sun and Wang (2018) documented that the interannual variability of summer precipitation over the TRS region is essentially modulated by an Eurasian wave-train associated with summer NAO; in addition, Indian Ocean warming occurring during an El Niño-decaying summer may also play a role in modulating the interannual variability of summer precipitation over the TRS region.

During past decades, relationships between East Asian climate and ENSO, NAO, Arctic Oscillation (AO), and SSTs over the Indian and Atlantic Oceans have undergone changes for a variety of reasons (Wang 2002; Sun and Wang 2012, 2015; Wang and He 2012; He and Wang 2013; Han et al. 2017). These changes of teleconnection relationship reflect changes in regimes of East Asian climate variability. For instance, Sun and Wang (2012) suggested that the summer NAO pattern underwent an interdecadal change after the late 1970s that generated an anomalous dipole pattern in the atmosphere over East Asia and thus had a significant effect on East Asian climate variability after the late 1970s. Han et al. (2017) proposed that winter precipitation occurring over northeastern China was largely modulated by an Eurasian wave pattern stimulated by anomalous Indian Ocean SSTs from 1961 to 1990 whereas it was significantly influenced by Rossby waves induced by anomalous North Atlantic SSTs from 1996 to 2013.

On the basis of aforementioned studies, two critical questions arise: how has the relationship between summer precipitation in the TRS region and its influencing factors changed over past decades, and why has this occurred? To address these questions, the present study examines variations in the correlation between summer (June–July–August, JJA) precipitation in the TRS region and global climate regimes including NAO, AO, ENSO, and global SSTs for past decades, and it investigates corresponding underlying mechanisms.

2 Data and methods

2.1 Data

The domain of the TRS region is defined as (31.5°–36.5°N, 89.5°–102.5°E) in this study, as shown in Fig. 1. Precipitation data are derived from monthly CN05.1 gridded data (0.25° × 0.25°) for 1961–2014. The CN05.1 data is constructed based on over 2400 stations across China, including over 40 stations positioned in the TRS region (Wu and Gao 2013). Sun and Wang (2018) showed that CN05.1 data results are consistent with station, Global Precipitation Climatology Project (GPCP), and Climatic Research Unit (CRU) data results regarding TRS precipitation variability.

The monthly reanalysis data (2.5° × 2.5°) used in this study are derived from the National Centers for Environmental Prediction (NCEP), including data of surface pressure, zonal and meridional winds, specific humidity, geopotential height, and vertical velocities at eight pressure

levels of 1000–300 hPa (Kalnay et al. 1996). SST data are derived from the NOAA Extended Reconstructed SST V4 (2.5° × 2.5°) (Huang et al. 2015). AO, NAO, and Niño 3.4 indices are derived from the NOAA Climate Prediction Center (https://www.esrl.noaa.gov/psd/data/climateindices/list/). Following Wang (2002), anomalies of areal mean 850 hPa wind speed for the region (20°–40°N, 110°–125°E) are used as an index to measure the strength of the EASM.

2.2 Methods

Two indices for ENSO are used in this study: the Niño 3.4 index and the Niño 3.4 tendency index. The Niño 3.4 tendency index is calculated from the Niño 3.4 index for the concurrent summer (JJA) minus the Niño 3.4 index for the preceding winter (December–January–February, DJF). The Niño 3.4 tendency index is used to denote the tendency of ENSO state from the preceding winter to the summer, which is critical to global summer climates (Wu et al. 2009; Xie et al. 2009; Chen et al. 2012). A negative anomaly in the Niño 3.4 tendency index denotes the occurrence of an El Niño-decaying summer, while a positive anomaly in the Niño 3.4 tendency index denotes the occurrence of a La Niña-decaying summer.

To investigate the change in the relationship between TRS summer precipitation and the global climate system, a running correlation with a 21-year window is applied to examine variations in the correlation between the time series of areal mean summer precipitation for the TRS region and time series of associated influencing factors for past decades. This study focuses on the relationship of interannual variability of TRS summer precipitation with the global climate system. Hence, for every 21-year window, the time series for areal mean summer precipitation for the TRS region and associated influencing factors are detrended to remove linear trends and to retain interannual variations found within this window before the correlation is computed. In addition, to examine the robustness of the results of the detrended time series, 9-year high-pass filtered time series are used to compute the 21-year running correlation with a Lanczos filter (Duchon 1979), the results of which largely resemble the results of detrended time series. Particularly for the filtered time series, the first and last five values of the time series become missing values after 9-year high-pass filtering. Thus, the first and last five 21-year windows have missing value(s), and corresponding correlation coefficients are computed based on a 21-year window with missing value(s). The analysis and discussion presented in this study are mainly based on the results of detrended time series given that the results of high-pass filtered time series reveal sensitivities to the threshold for high-pass filtering and given that high-pass filtering results in missing values for the first/last several years of time series.

Climate anomalies regressed on the standardized time series for areal mean TRS summer precipitation are computed via a linear regression analysis to denote climate anomalies associated with the interannual variability of TRS summer precipitation, including 500 hPa geopotential height anomalies, vertically integrated water vapor transport (WVT) anomalies, vertically integrated atmospheric moisture anomalies, 850 hPa wind anomalies, 500 hPa vertical velocity anomalies, and SST anomalies. The vertically integrated WVT and atmospheric moisture are computed from a vertical integration of water vapor flux and specific humidity from surface pressures to the 300 hPa pressure level, respectively, using the method developed by Sun et al. (2011). Climate anomalies regressed on the standardized time series for NAO, AO, western Indian Ocean SST, ENSO, and the EASM are also computed to represent corresponding climate anomalies associated with these factors.

Computations are applied to examine the sensitivity of results to the domain of the TRS region, denoting that a minor change in the domain for the TRS region should not lead to a major change in the results. For instance, the time series for areal mean summer precipitation for domain (31.5°–36.5°N, 89.5°–102.5°E) are largely consistent with time series for areal mean summer precipitation for domains (31.5°–36.5°N, 90.5°–101.5°E) and (30.5°–35.5°N, 89.5°–102.5°E) with correlation coefficients of 0.99 and 0.93 at the 99% confidence level, respectively.

3 Regimes of TRS summer precipitation and enhanced teleconnection relationships

3.1 Overview of TRS summer precipitation regimes

In Sun and Wang (2018), two major factors are suggested to influence the interannual variability of TRS summer precipitation from 1979 to 2014, including an Eurasian wave-train associated with summer NAO and an anomalous anticyclone over the Bay of Bengal during an El Niño-decaying summer. In the current study, to provide an overview of climate regimes associated with TRS summer precipitation, Fig. 2 shows climate anomalies associated with the interannual variability of TRS summer precipitation for the last 24 years (1991–2014). The 500 hPa geopotential height and vertically integrated WVT anomalies show impacts of the Eurasian wave-train associated with summer NAO, which induces an anomalous low over the TRS region and southwesterly WVT anomalies towards the TRS region (Fig. 2a). This wave-train somewhat resembles the conventional Eurasian (EU) pattern, which is suggested to be driven by anomalous North Atlantic SSTs (Liu et al. 2014b). However, the EU teleconnection pattern is generally observed during the boreal

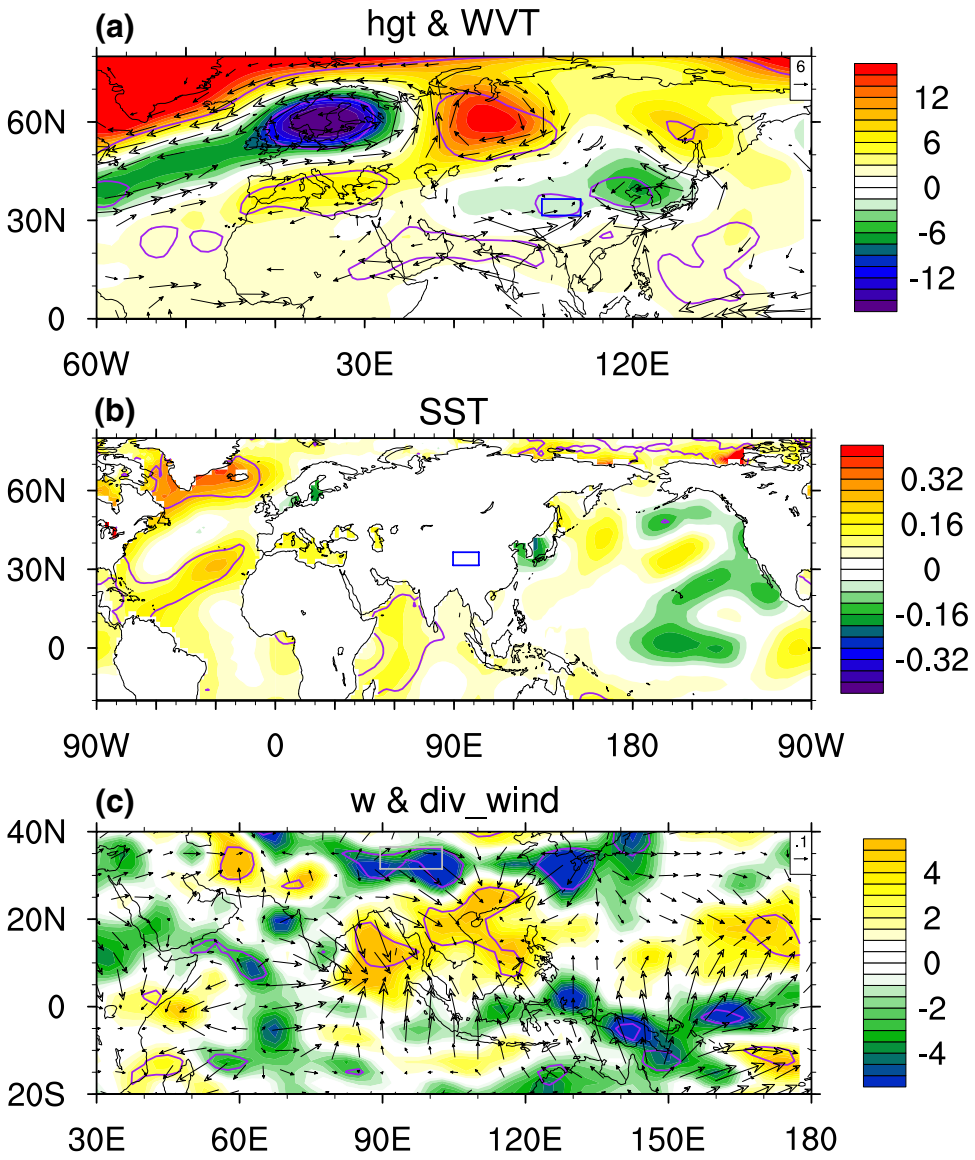

Fig. 2 Anomalies of **a** 500 hPa geopotential height (colored shading, unit: gpm) and vertically integrated WVT (vectors, unit: kg m^{-1} s^{-1}), **b** SST (colored shading, unit: °C), and **c** 500 hPa vertical velocity (unit: Pa s^{-1}) and 200 hPa divergent wind (vectors, unit: m s^{-1}) regressed on the detrended and standardized time series of areal mean TRS summer precipitation for 1991–2014. Purple contours shown in **a, b**, and **c** denote the 95% confidence level for anomalies of 500 hPa geopotential height, SST, and 500 hPa vertical velocity, respectively. Vectors shown in **a** only reflect WVT anomalies significant at the 95% confidence level. The domain of the TRS region is denoted by a blue rectangle in **a** and **b** and by a grey rectangle in **c**

winter. The mechanism underlying this Eurasian wave-train during the boreal summer may differ from that of the winter EU pattern. Correspondingly, the SST anomalies follow a meridional tripole pattern in the North Atlantic known as a pattern coupled with NAO (Rodwell et al. 1999; Robertson et al. 2000; Czaja and Frankignoul 2002; Hurrell et al. 2003). In addition, the SST anomalies exhibit a warming western Indian Ocean (Fig. 2b).

During the summer, warming in the western Indian Ocean can induce anticyclonic WVT anomalies over the Bay of Bengal and can particularly cause southwesterly WVT anomalies towards the TRS region as a result of a tropical Kelvin wave response to western Indian Ocean warming (Wu et al. 2009; Xie et al. 2009; Sun and Wang 2018). In addition, this study shows that in response to western Indian Ocean warming, convection is strengthened in the troposphere, and divergent wind anomalies form in the upper-level troposphere over the western Indian Ocean (Fig. 2c). Accordingly, compensatory subsidence anomalies and upper-level convergence anomalies form over the Bay of Bengal (Fig. 2c), contributing to an anomalous high and an anomalous anticyclone forming over the Bay of Bengal (Fig. 2a).

In addition to the Eurasian wave-train associated with NAO and the anomalous anticyclone forming over the Bay of Bengal, an anomalous high forming over the western North Pacific (WNP) also contributes to TRS summer precipitation by inducing southwesterly WVT anomalies along its northwestern flank (Fig. 2a). Studies show that the anomalous high forming over the WNP during the summer can be induced by tropical Indian Ocean warming and/or strengthened convective activity over the Maritime Continent (Huang 1992; Wu et al. 2009; Xie et al. 2009; Sun and Wang 2015). The tropical Indian Ocean warms up during

an El Niño event due to an atmospheric bridge effect of ENSO and this warming peaks during spring and persists through the subsequent summer as El Niño decays (Schott et al. 2009; Xie et al. 2009). The warming in the tropical Indian Ocean during summer is found to spur easterly wind anomalies over the tropical western Pacific, causing an anticyclonic wind shear and resulting in an anomalous anticyclone over the WNP, which can be considered a delayed effect of preceding winter El Niño (Wu et al. 2009; Xie et al. 2009). Strengthened convective activity over the Maritime Continent may also contribute to an anomalous high forming over the WNP via the so-called "Pacific-Japan (PJ) pattern" or "East Asia-Pacific (EAP) pattern" (Nitta 1987; Huang 1992; Sun and Wang 2015), stimulating a meridional wavetrain characterized by anomalous descending motion over WNP and anomalous ascending motion over eastern China and Japan. As shown in Fig. 2c, convection anomalies over the Maritime Continent and subsidence anomalies over WNP and South China Sea and convection anomalies over eastern China and Japan are observed to be associated with TRS summer precipitation, which however are mostly below the 95% confidence level, implying an effect of convective activity over the Maritime Continent inferior to effects of other factors such as summer NAO and western Indian Ocean warming on TRS summer precipitation as mentioned before. On the other hand, these anomalies are generally at the 80% confidence level. Thus, the relationship between convective activity over the Maritime Continent and TRS summer precipitation deserves an investigation. Essentially, tropical Indian Ocean warming meditates effects of preceding winter El Niño on the anomalous anticyclone over WNP during the summer, while convection anomalies over the Maritime Continent during the summer are associated with both preceding winter El Niño events and concurrent tropical Pacific SSTs (Wang et al. 2000; Yang et al. 2007; Wu et al. 2009; Sun and Wang 2015; Xue and Zhao 2017). For instance, during an El Niño-decaying summer or a summer of tropical central-eastern Pacific cooling, convective activity is strengthened over the Maritime Continent due to an enhanced Walker circulation (Wu et al. 2009; Sun and Wang 2015; Xue and Zhao 2017).

Of particular note are the insignificant SST anomalies observed in the tropical central and eastern Pacific (Fig. 2b), which appear to imply the presence of an insignificant relationship between TRS summer precipitation and the tropical Pacific SSTs for the concurrent summer of 1991–2014. However, our results indicate that for 1979–2014, there is a significant relationship between TRS summer precipitation and tropical central Pacific SSTs of the concurrent summer (figure not shown). The difference between the results for the two periods may be mainly attributed to the fact that the relationship between TRS summer precipitation and concurrent tropical Pacific SSTs varies with time. Hence, the impact of concurrent summer tropical Pacific SSTs on TRS summer precipitation should not be overlooked.

Thus, the interannual variability of TRS summer precipitation is modulated by a variety of factors including the EASM, NAO, Indian Ocean SST, and ENSO. It should be noted that the influences of these factors are not independent but that they are internally linked. The interannual variability of the EASM is affected by ENSO, Indian Ocean SST, and NAO but is not necessarily determined by these factors because the EASM is essentially influenced by the land-sea thermal contrast.

3.2 Enhanced teleconnection relationships

Figure 3 shows the 21-year-window running correlation between the time series of areal mean TRS summer precipitation and time series of concurrent summer NAO, AO, western Indian Ocean SST, EASM index, Niño 3.4 index, and Niño 3.4 tendency index for past decades. According to Fig. 2b, the time series for western Indian Ocean SST is calculated from the areal mean SST for the region covering (20°S–20°N, 40°–80°E). As shown in Fig. 3a, the correlation between TRS summer precipitation and NAO persistently increased over past decades with an insignificant correlation found before the 1980s and with a significant negative correlation found after the 1990s. The relationship between TRS summer precipitation and AO undergoes a gradual shift from a positive correlation prior to the 1980s to a significant negative correlation after the 1990s (Fig. 3b). Similarly, western Indian Ocean SST shows a persistently increasing correlation with TRS summer precipitation for past decades with an insignificant correlation found prior to the 1990s and a significant positive correlation occurring afterwards (Fig. 3c). The results of detrended and 9-year high-pass filtered time series show a strong consistency for the abovementioned NAO-, AO-, and western Indian Ocean-associated running correlations.

By contrast, the running correlation between the time series for TRS summer precipitation and the EASM index presents an inconsistency between results of the detrended time series and results of the 9-year high-pass filtered time series (Fig. 3d). For the detrended time series, running correlation coefficients between the time series for TRS summer precipitation and the EASM index increase after the 1980s and decline to smaller values in more recent years, falling below the 95% confidence level for the whole period. On the other hand, for the 9-year high-pass filtered time series, running correlation coefficients between the time series for TRS summer precipitation and the EASM index increase to relatively large values significant at the 95% confidence level after the 1980s and increase further in recent years. To examine this inconsistency, two windows for the detrended time series and 9-year high-pass filtered time series are

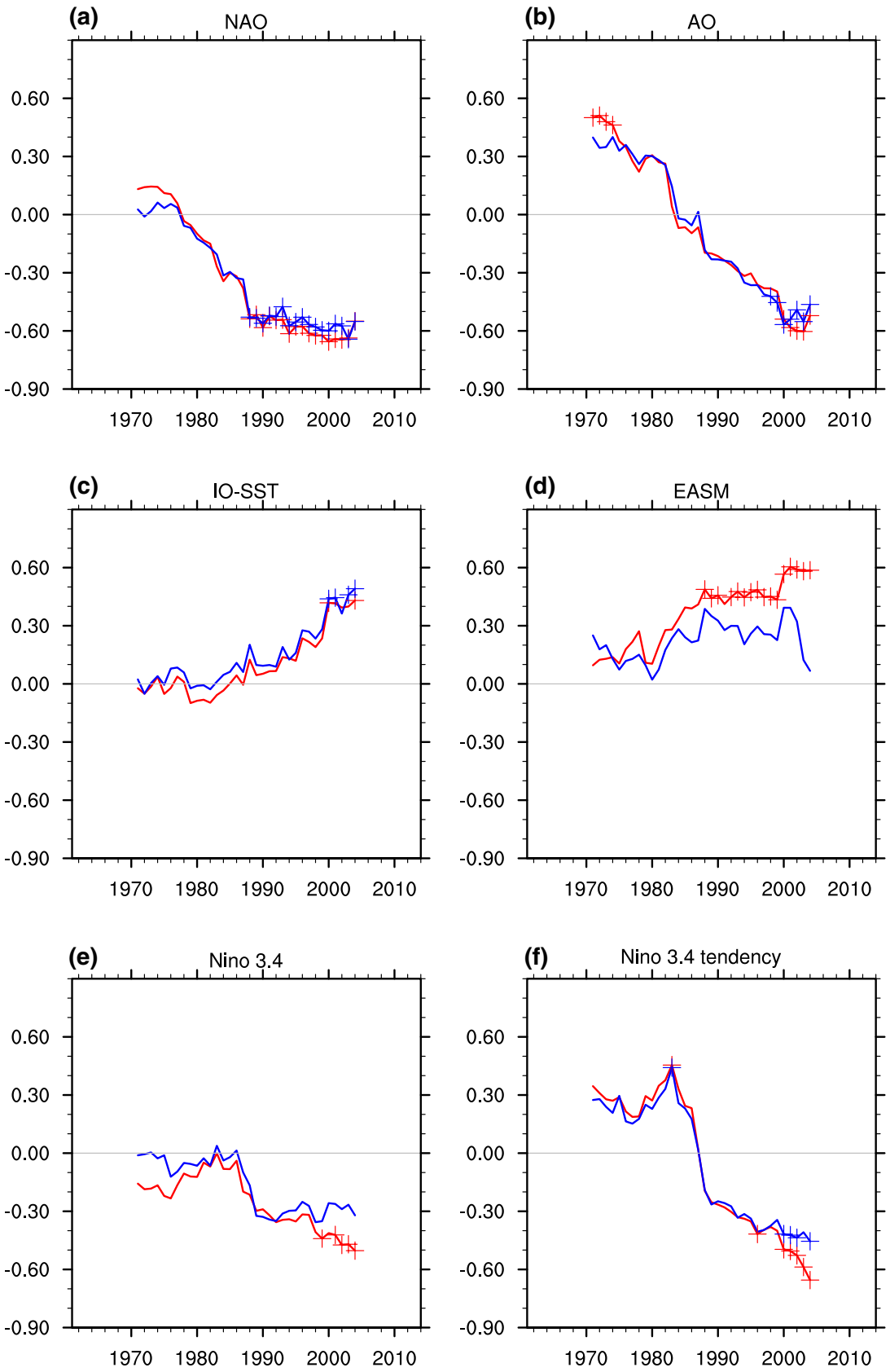
(a)
NAO
(b)
AO
(c)
IO-SST
(d)
EASM
(e)
Nino 3.4
(f)
Nino 3.4 tendency
0.60
0.30
0.00
-0.30
-0.60
-0.90
1970
1980
1990
2000
2010

◂**Fig. 3** Running correlation coefficients between the time series for areal mean TRS summer precipitation and the time series for the **a** NAO index, **b** AO index, **c** areal mean western Indian Ocean SST for (20°S–20°N, 40°–80°E), **d** EASM index, **e** Niño 3.4 index, and **f** Niño 3.4 tendency index with a 21-year window. Blue lines represent results of the detrended time series. Red lines represent results of the 9-year high-pass filtered time series. Correlation coefficients at the 95% confidence level are marked with "+" symbols

compared: windows 1985–2005 and 1994–2014. It is indicated that time series for TRS summer precipitation and for the EASM index are mainly consistent in quasi-biennial oscillation, while the quasi-biennial oscillation is more significant in the 9-year high-pass filtered time series than in the detrended time series. In addition, interannual variations in TRS summer precipitation and in the EASM are out-of-phase after 2010, and this is reflected in the detrended time series but not in the 9-year high-pass filtered time series because the last five values of the 9-year high-pass filtered time series are missing values. Accordingly, a discrepancy is found between results for the detrended and 9-year high-pass filtered time series.

Regarding ENSO, the summer Niño 3.4 index shows an increased correlation with concurrent TRS summer precipitation after the 1980s, which is measured at (below) the 95% confidence level for recent years in the 9-year high-pass filtered (detrended) time series (Fig. 3e). The Niño 3.4 tendency index shows a significantly negative correlation with TRS summer precipitation for recent years and an insignificant correlation for the period preceding the 1990s (Fig. 3f). For both the detrended time series and the 9-year high-pass filtered time series, the correlation coefficient between the Niño 3.4 tendency index and TRS summer precipitation is larger than the correlation coefficient between the Niño 3.4 index and TRS summer precipitation for recent years, revealing a closer relationship between TRS summer precipitation and ENSO tendency from the preceding winter to the summer than with concurrent summer tropical Pacific SSTs for recent years.

This raises the following question: why has the relationship between TRS summer precipitation and global climate system been enhanced? Changes in the correlation between TRS summer precipitation and its influencing factors are mostly gradual changes with the exception of a relatively rapid change occurring in the correlation with the Niño 3.4 tendency index for the 1980s, suggesting that the influence of these factors on TRS summer precipitation has varied gradually rather than suddenly over past decades. In consideration of these gradual changes, the following discussions offers insight into the above question by comparing atmospheric circulation and SST anomalies associated with NAO, EASM, western Indian Ocean SST, and Niño 3.4 tendency index for two periods, an earlier period 1961–1980 and a later period 1991–2014.

4 Enhanced connections to NAO

Figure 4 shows the 500 hPa geopotential height and vertically integrated WVT anomalies associated with a negative-phase summer NAO for 1961–1980 and 1991–2014. It is indicated that for 1961–1980, a negative-phase NAO mode is associated with a meridional see-saw pattern of atmospheric circulation anomalies occurring over the North Atlantic and Europe, with no observable Eurasian wave-train patterns associated with the NAO mode and limited impacts of NAO on downstream regions such as central Asia, western China, and the Tibetan Plateau, including the TRS region (Fig. 4a). By contrast, for 1991–2014, a negative-phase NAO mode is characterized by a zonal wave pattern forming over the North Atlantic and Europe with an anomalous high (low) found over Greenland (northern Europe), which is associated with a southeastward-propagating wave-train forming over Eurasia and resulting in an anomalous low over the TRS region and southwesterly WVT anomalies towards the TRS region (Fig. 4b).

The main difference in NAO-associated atmospheric circulation anomalies found between the two periods is a southeastward-propagating wave-train forming over Eurasia during the latter period. What caused this difference? To illustrate the source of the anomalous wave-train, the horizontal wave activity flux associated with 500 hPa geopotential height anomalies is computed (Plumb 1985). As shown in Fig. 5b, for 1991–2014, the wave activity flux of this anomalous Eurasian wave-train originates from the Hudson Bay-Davis Straight (HB-DS) region located adjacent to the anomalous high center over southwestern Greenland (Fig. 4b). Correspondingly, significant positive atmospheric moisture anomalies are distributed across the troposphere over the HB-DS region (Fig. 5b). In contrast, for 1961–1980, a negative-phase NAO mode is associated with relatively small wave activity flux and with less significant atmospheric moisture anomalies occurring over the HB-DS region (Fig. 5a). Thus, it can be inferred that atmospheric activity occurring over the HB-DS region and the adjacent anomalous warm high over Greenland play a key role in stimulating the anomalous wave-train over Eurasia whereby a strong (weak) anomalous warm high over Greenland is associated with a significant (insignificant) Eurasian wave-train, as shown in Fig. 4b (Fig. 4a).

The aforementioned atmospheric moisture anomalies may have an important impact on the formation of a strong anomalous warm high over Greenland. Under a negative-phase NAO, southeasterly WVT anomalies prevail over the HB-DS region, resulting in the presence of warmer and moister air over this region. The increased atmospheric moisture can boost latent heat release resulting from

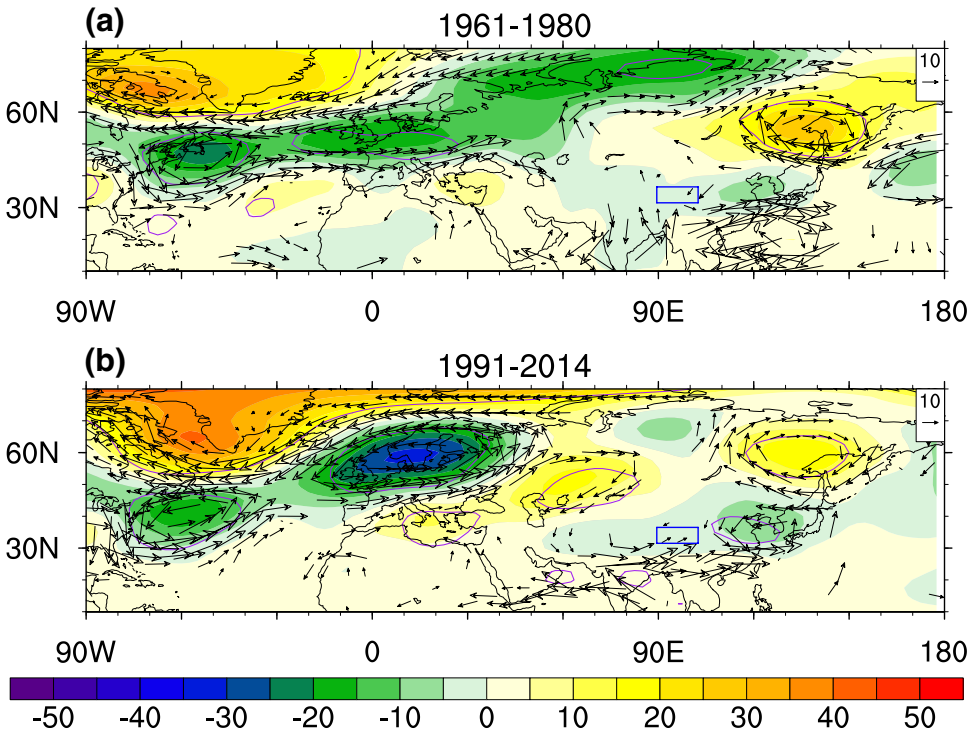

Fig. 4 Anomalies of 500 hPa geopotential height (colored shading, unit: gpm) and vertically integrated WVT (vectors, unit: kg m^{-1} s^{-1}) regressed on the detrended and standardized time series for the sign-reversed NAO index for **a** 1961–1980 and **b** 1991–2014. Purple contours denote the 95% confidence level of 500 hPa geopotential height anomalies. Vectors are only shown for WVT anomalies significant at the 90% confidence level. The domain of the TRS region is denoted by a blue rectangle (the same for the subsequent figures)

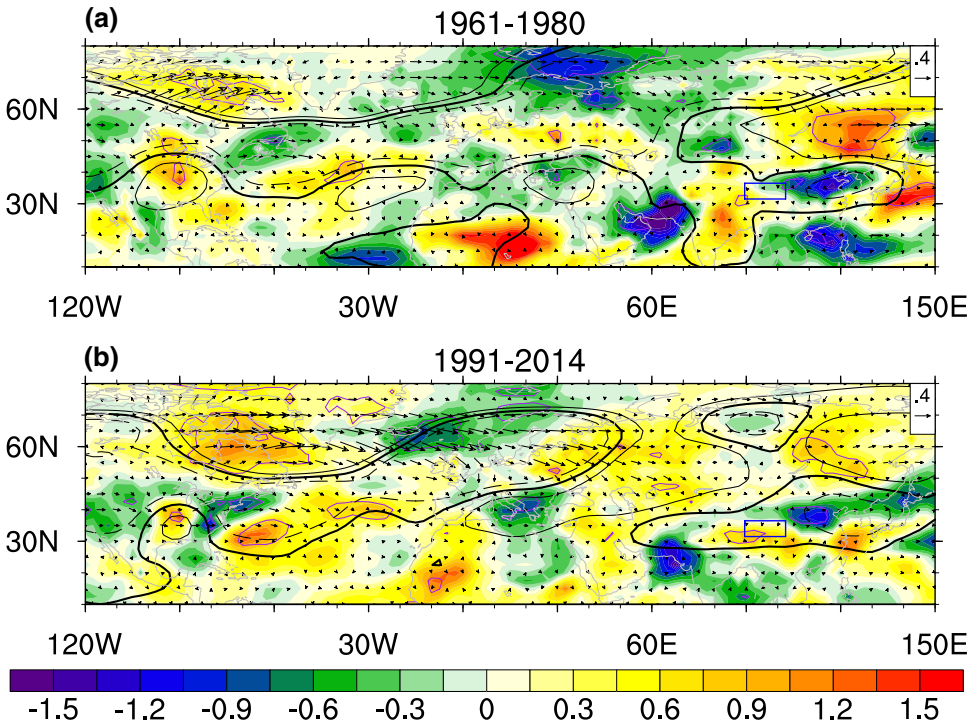

Fig. 5 Anomalies of vertically integrated atmospheric moisture (colored shading, unit: kg m^{-2}) and 500 hPa geopotential height (black contours, unit: gpm) regressed on the detrended and standardized time series for the sign-reversed NAO index for **a** 1961–1980 and **b** 1991–2014. The thick black contour denotes the zero line, and the thin solid (dashed) line denotes a positive (negative) value at an interval of 5 gpm. The vectors denote the wave activity flux associated with 500 hPa geopotential height anomalies (unit: m^{-2} s^{-2}). Purple contours denote the 95% confidence level of vertically integrated atmospheric moisture anomalies

climatic ascending motion over the HB-DS region during the summer, contributing to anomalous warming over the HB-DS region and over Greenland (Fig. 4b). More importantly, as shown in Fig. 6b, the boosted latent heating can strengthen convective activity over the HB-DS region, which may induce compensatory subsidence anomalies over southern Greenland and hence intensify the anomalous high over Greenland.

Due to global warming and Arctic amplification, the atmospheric moisture content has been increased around

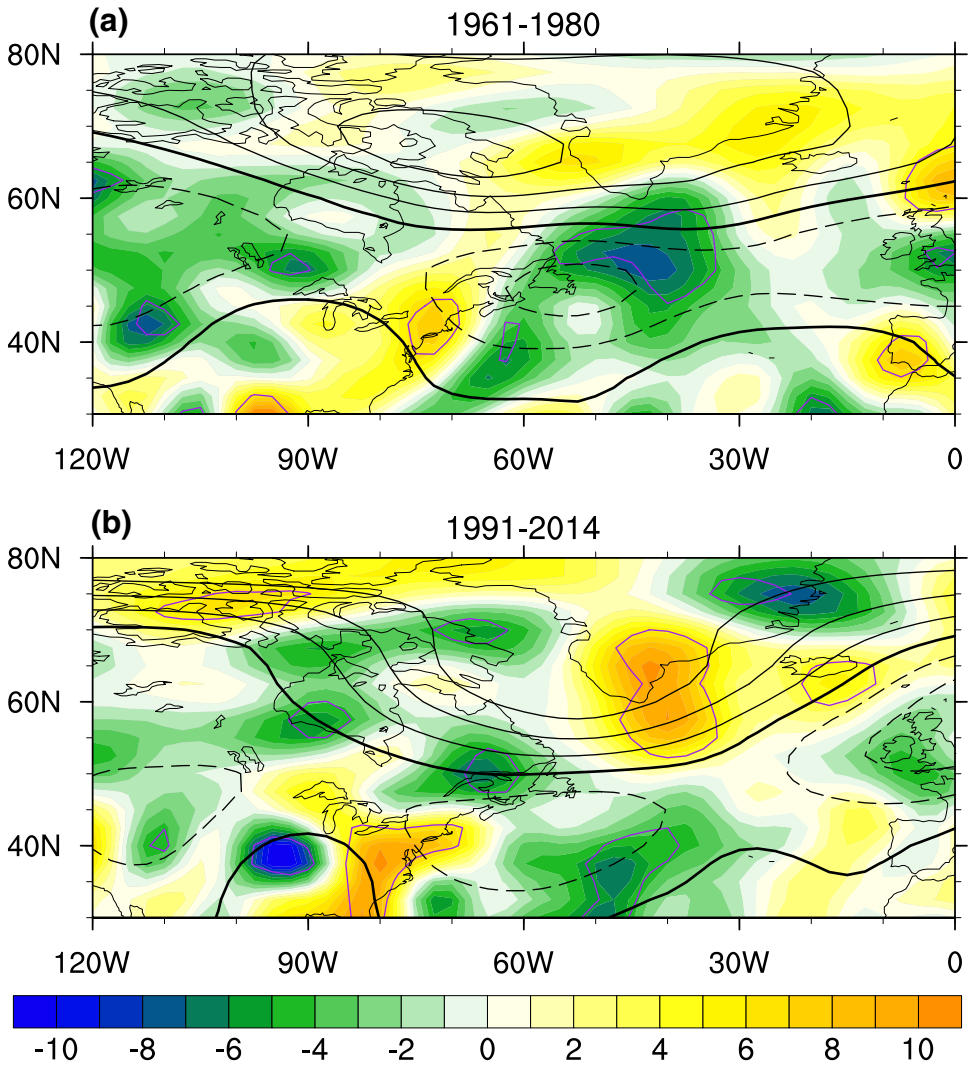

Fig. 6 Anomalies of 500 hPa vertical velocity (colored shading, unit: Pa s^{-1}) and 500 hPa geopotential height (black contours, unit: gpm) regressed on the detrended and standardized time series of the sign-reversed NAO index for **a** 1961–1980 and **b** 1991–2014. The thick black contour denotes the zero line, and the thin solid (dashed) contour denotes a positive (negative) value at an interval of 10 gpm. Purple contours denote the 95% confidence level of 500 hPa vertical velocity anomalies

the globe over past decades, including those of the Arctic region (Held and Soden 2006; Francis and Vavrus 2012). Hence, the latent heating of atmospheric moisture has had an increasingly more important impact on the anomalous warm high over Greenland during negative-phase NAO summers as the atmospheric moisture increases, which may be a key cause of the formation of zonal wave patterns over the North Atlantic and Europe and of an associated anomalous wave-train forming over Eurasia (Fig. 4b). Figure 7 shows a schematic diagram of the different effects of latent heating of atmospheric moisture on the anomalous warm high over Greenland associated with negative-phase NAO for 1961–1980 and 1991–2014. For 1961–1980 (Fig. 7a), southeasterly WVT anomalies over the HB-DS region are relatively minor during negative-phase NAO summers, which is partially due to relatively small specific humidity observed over the Arctic region. These weak anomalous moisture transport branches have a limited impact on the atmospheric moisture over the HB-DS region, which cannot boost the latent heating significantly and thus exerts limited effects on convective activity over the HB-DS region and on the anomalous warm high over Greenland. In contrast, for 1991–2014 (Fig. 7b), southeasterly WVT anomalies over the HB-DS region are significant during negative-phase NAO summers, which is partially due to increased atmospheric moisture observed over the Arctic region under global warming. This strong anomalous moisture transport spurs a significant effect of latent heating over the HB-DS region, strengthening convective activity over the HB-DS region. These convection anomalies further induce compensatory subsidence anomalies over southern Greenland, intensifying the anomalous high over Greenland. Consequently, a strengthened anomalous warm high forms over Greenland. This strengthened anomalous warm high in turn generates an intensified anticyclonic WVT regime and enhances southeasterly moisture transport over the HB-DS region as positive feedback to the boosted latent heating over the HB-DS region. Accordingly, strengthened convective activity over

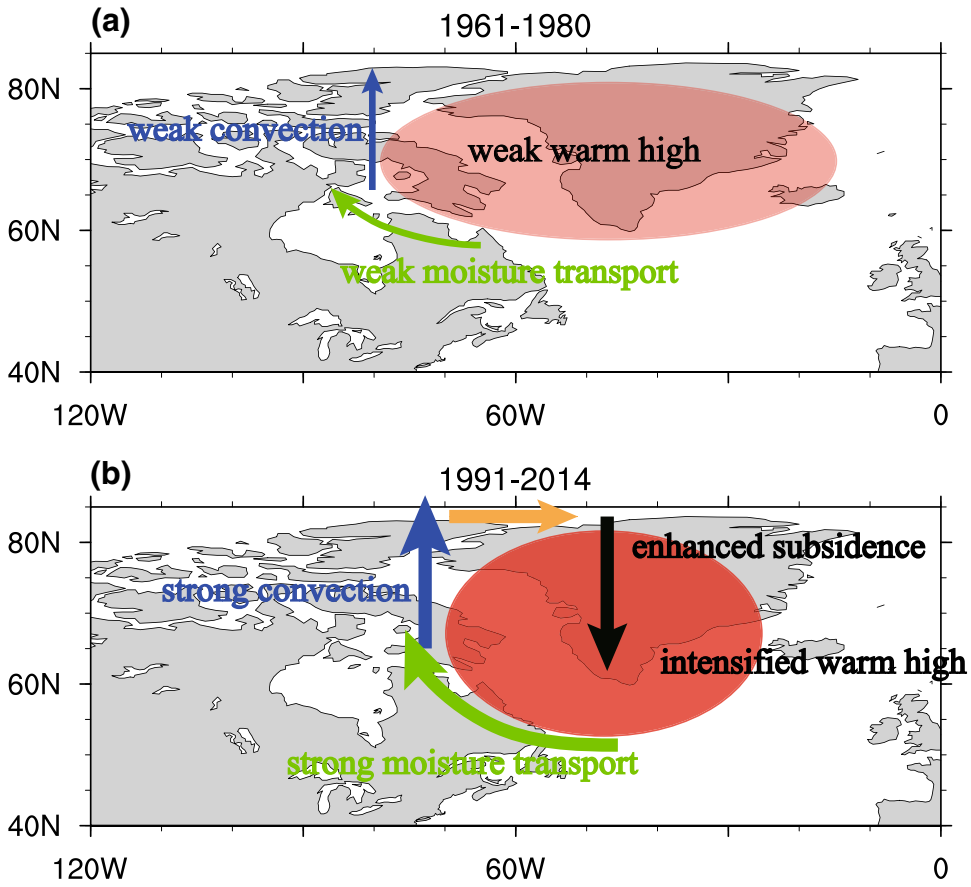

Fig. 7 Schematic diagram of the effect of latent heating of atmospheric moisture over the HB-DS region associated with negative-phase summer NAO for **a** 1961–1980 and **b** 1991–2014. For **a** 1961–1980, anomalous southeasterly moisture transport over the HB-DS region and associated latent heating are relatively weak and have little influence on the anomalous warm high over Greenland. For **b** 1991–2014, southeasterly moisture transport over the HB-DS region and associated latent heating are strong, causing strengthened convection over the HB-DS region and compensatory subsidence anomalies over Greenland

the HB-DS region and an intensified anomalous warm high over Greenland occur during negative-phase NAO summers whereby a wave-train is stimulated and propagated southeastward.

Considering that increases in SST over the HB-DS region may also contribute to overlying convective activity, SST anomalies and surface latent heat flux and sensible heat flux anomalies over the HB-DS region are also examined and present limited significance of below the 95% confidence level. Thus, air–sea interactions occurring over the HB-DS region are likely not a key factor related to this issue.

5 Enhanced connections to the western Indian Ocean

Figure 8 shows anomalies of 500 hPa geopotential height and vertically integrated WVT regressed on the time series of areal mean SST for the western Indian Ocean (20°S–20°N, 40°–80°E) for the summer of 1961–1980 and 1991–2014. It is shown that for 1991–2014, warming in the western Indian Ocean is associated with an anomalous high over the Bay of Bengal and South China Sea, which induces southwesterly WVT anomalies towards the TRS region and which thus contributes to summer precipitation over the TRS region (Fig. 8b). For 1961–1980, warming in the western Indian Ocean is associated with a less significant anomalous high over the Bay of Bengal and South China Sea; hence, less significant WVT anomalies are induced towards the TRS region (Fig. 8a).

It has been suggested that warming in the tropical Indian Ocean can induce/maintain an anomalous anticyclone over the WNP during an El Niño-decaying summer via a Kelvin wave-induced Ekman divergence mechanism (Wu et al. 2009; Xie et al. 2009). Strengthened convection associated with warming in the tropical Indian Ocean stimulates a Kelvin wave response over the western tropical Pacific, causing low-level easterly wind anomalies over the western tropical Pacific and an anticyclonic wind shear over the WNP, which further induce anomalous divergence and subsidence in the planetary boundary layer over the WNP. Subsidence anomalies in the planetary boundary layer suppress convection over the WNP and hence cause subsidence anomalies in the troposphere over the WNP, generating an anomalous high and anticyclonic regime over the WNP. Warming in the western Indian Ocean may have similar effects and induces an anomalous high over the Bay of Bengal and South China Sea via the abovementioned Kelvin wave-induced Ekman divergence mechanism. However, how can western Indian Ocean warming have different effects during different periods?

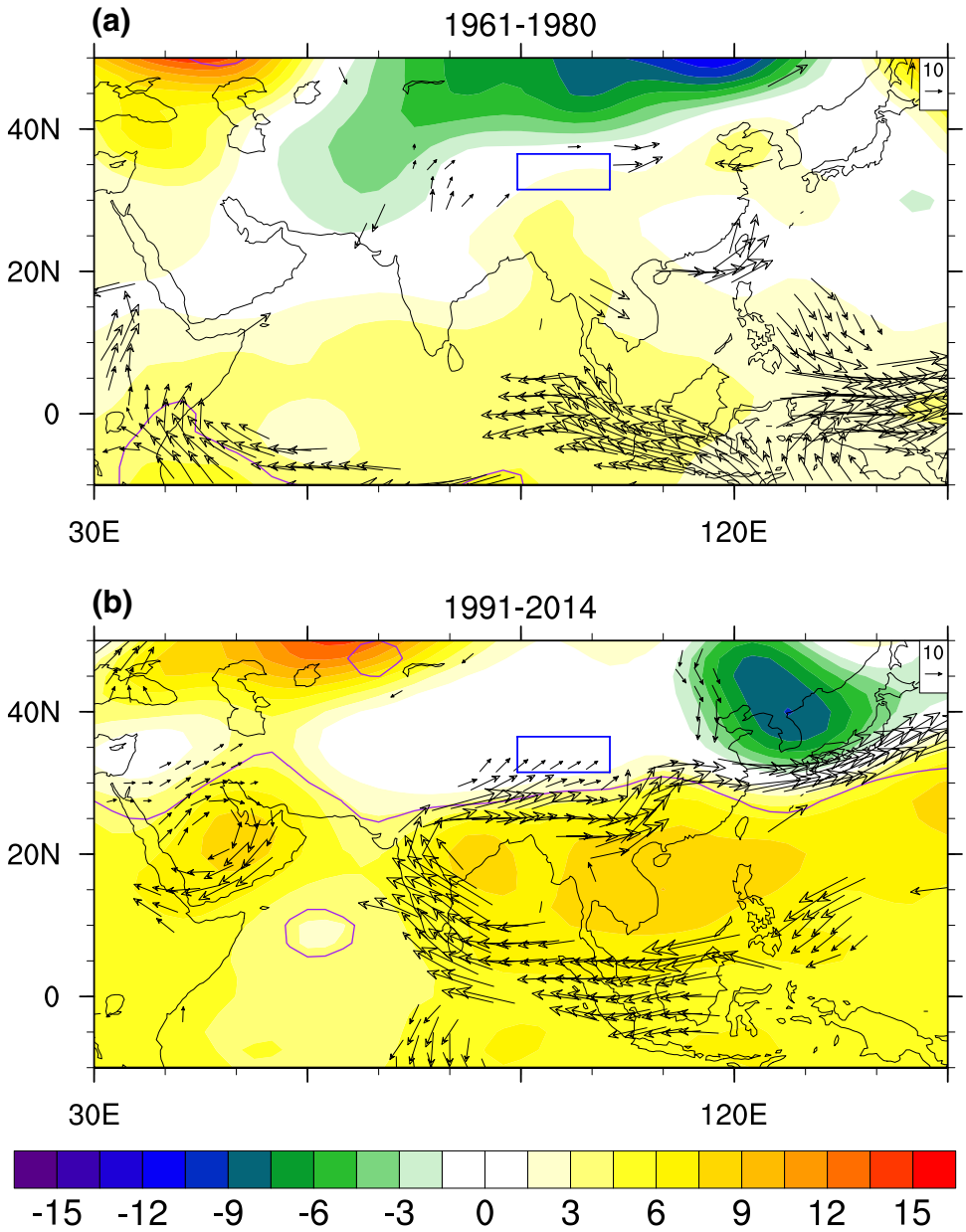

Fig. 8 Anomalies of 500 hPa geopotential height (colored shading, unit: gpm) and vertically integrated WVT (vectors, unit: kg m^{-1} s^{-1}) regressed on the detrended and standardized time series for areal mean SST over the western Indian Ocean (20°S–20°N, 40°–80°E) for **a** 1961–1980 and **b** 1991–2014. Purple contours denote the 95% confidence level of 500 hPa geopotential height anomalies. Vectors are only shown for WVT anomalies significant at the 90% level

To answer this question, SST anomalies and 850 wind anomalies regressed on the times series of areal mean SST for the western Indian Ocean (20°S–20°N, 40°–80°E) are computed for the two periods. As shown in Fig. 9a, for 1961–1980, warming of the western Indian Ocean is found with a warming center positioned south of the equator. As a Kelvin wave response to enhanced convection over the western Indian Ocean, low-level easterly wind anomalies are caused over the tropical Indian Ocean and are mainly distributed to south of the equator due to the warming center south of the equator. Accordingly, less significant wind anomalies are caused to the north of the equator and the climate regime over the Bay of Bengal and TRS region is not significantly affected. In contrast, for 1991–2014, western Indian Ocean warming occurs with a warming center over the Arabian Sea north of the equator (Fig. 9b). Correspondingly, low-level easterly wind anomalies are caused over the tropical Indian Ocean and western Pacific as a Kelvin wave response to strengthened convection over the western Indian Ocean, which are mainly distributed north of the equator due to the warming center positioned north of the equator. These easterly wind anomalies cause an anticyclonic wind shear and an anomalous high in the troposphere over the Bay of Bengal and South China Sea (Fig. 9b), inducing southwesterly WVT anomalies towards the TRS region (Fig. 8b). In addition, different Pacific SST anomalies are associated with the warming of the western Indian Ocean in the two periods. For 1961–1980, the warming of the western Indian Ocean

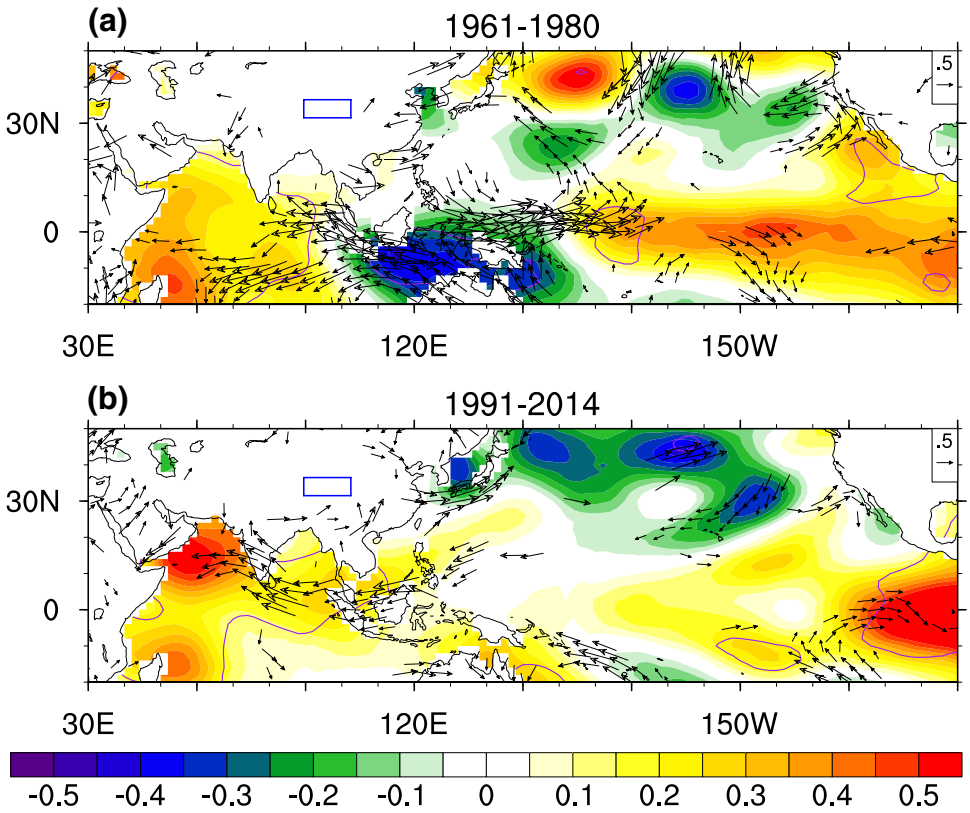

Fig. 9 Anomalies of SST (colored shading, unit: °C) and 850 hPa wind (vectors, unit: m s^{-1}) regressed on the detrended and standardized time series for areal mean SST over the western Indian Ocean (20°S–20°N, 40°–80°E) for **a** 1961–1980 and **b** 1991–2014. Purple contours denote the 95% confidence level of SST anomalies. Vectors are only shown for 850 hPa wind anomalies significant at the 90% confidence level

occurs concurrently with cooling in the tropical Indo-Pacific region and with warming in the tropical central and eastern Pacific, which causes low-level westerly wind anomalies over the tropical western Pacific (Fig. 9a). These westerly wind anomalies are not conducive to an anticyclonic wind shear over the South China Sea; also, descending motion anomalies over the Maritime Continent spurred by the cooling of the tropical Indo-Pacific region tend to induce an anomalous low over the South China Sea via PJ/EAP teleconnection pattern (Nitta 1987; Huang 1992). On the other hand, for 1991–2014, western Indian Ocean warming occurs concurrently with insignificant SST anomalies over the tropical Indo-Pacific region (Fig. 9b).

Thus, the shift in the warming center of the western Indian Ocean and the different concurrent Pacific SST anomalies may be central to why TRS summer precipitation has been more closely related to western Indian Ocean SSTs in recent decades. Further studies must be conducted to understand why the warming center over the western Indian Ocean has shifted and why Pacific SST anomalies forming concurrently with western Indian Ocean warming changed during the summer.

It should be noted that a basin-wide warming of the Indian Ocean generally occurs during an El Niño-decaying summer (Wu et al. 2009; Xie et al. 2009). However, western Indian Ocean warming may also occur during a summer of the positive-phase Indian Ocean Dipole (IOD) mode, which involves a contrasting relationship between western and eastern Indian Ocean SSTs on an interannual scale (Saji et al. 1999). The IOD is suggested to be independent of ENSO events (Saji et al. 1999). The warming of the western Indian Ocean during an El Niño-decaying summer and during a summer of the positive-phase IOD mode may have different climate effects extending beyond the scope of the present study.

6 Enhanced connections to ENSO

ENSO essentially modulates the East Asian summer climate via an anomalous anticyclone/cyclone forming over the WNP (Wang et al. 2000; Wu et al. 2009). Indian Ocean warming occurring during an El Niño-decaying summer can mediate effects of ENSO on this anomalous anticyclone/cyclone over the WNP (Wu et al. 2009; Xie et al. 2009). Convective activity over the tropical western Pacific and Maritime Continent can also affect the anomalous anticyclone/cyclone over the WNP via PJ/EAP teleconnection patterns (Nitta 1987; Huang 1992; Sun and Wang 2015). Since the effects of western Indian Ocean warming are clarified in Sect. 5, this section focuses on effects associated with convective activity over the Maritime Continent. Atmospheric circulation anomalies regressed on the Niño 3.4 index and Niño 3.4 tendency index are computed for 1961–1980 and

1991–2014. The results suggest that an enhanced latent heating of atmospheric moisture over the Maritime Continent has been central to the increased correlation found between TRS summer precipitation and the Niño 3.4 index/Niño 3.4 tendency index over recent years, as follows. Given the more significant correlation found between TRS summer precipitation and the Niño 3.4 tendency index for recent years, the following discussion is mainly based on results derived from the Niño 3.4 tendency index.

Figure 10 shows 500 hPa geopotential height and vertically integrated WVT anomalies regressed on the sign-reversed Niño 3.4 tendency index, which show climate anomalies for an El Niño-decaying summer. For 1991–2014, an El Niño-decaying summer is characterized by an anomalous high forming over the WNP and Indo-China Peninsula, which causes southwesterly WVT anomalies towards the TRS region along its northwestern flank, contributing to summer precipitation over the TRS region (Fig. 10b). In contrast, for 1961–1980, an El Niño-decaying summer is characterized by the presence of insignificant geopotential height anomalies over the WNP and by insignificant WVT anomalies found over the TRS

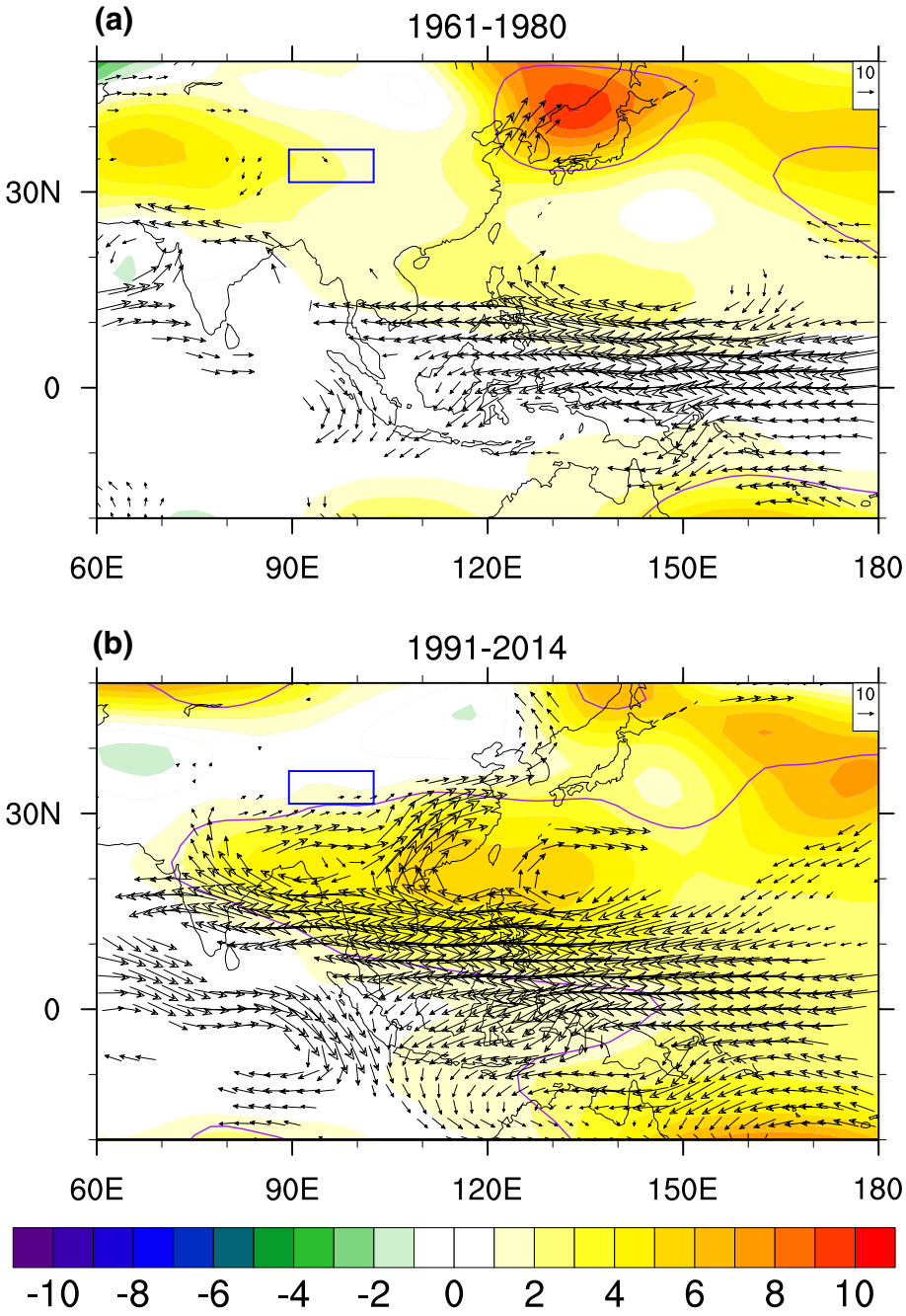

Fig. 10 Anomalies of 500 hPa geopotential height (colored shading, unit: gpm) and vertically integrated WVT (vectors, unit: kg m^{-1} s^{-1}) regressed on the detrended and standardized time series of the sign-reversed Niño 3.4 tendency index for **a** 1961–1980 and **b** 1991–2014. Purple contours denote the 95% confidence level of 500 hPa geopotential height anomalies. Vectors are only shown for WVT anomalies significant at the 90% confidence level

region (Fig. 10a). This difference is partially attributed to the difference in the meridional wave-train stimulated by convective activity over the Maritime Continent, i.e., PJ/EAP teleconnection patterns. As shown in Fig. 11a, b, during an El Niño-decaying summer, convection anomalies over the Maritime Continent are more significant for 1991–2014 (Fig. 11b) than for 1961–1980 (Fig. 11a) whereby a more significant PJ/EAP teleconnection pattern is stimulated for 1991–2014, generating more subsidence anomalies over the WNP. Strengthened convective activity over the Maritime Continent observed for 1991–2014 are largely attributed to enhanced latent heating of atmospheric moisture. As shown in Fig. 11c, d, more significant positive moisture anomalies are distributed over the Maritime Continent during El Niño-decaying summers of 1991–2014 than of 1961–1980, denoting more significant effects of latent heating occurring with convection over the Maritime Continent. Atmospheric circulation anomalies regressed on the sign-reversed Niño 3.4 index also highlight the importance of enhanced latent heating on enhanced convective activity over the Maritime Continent observed during summers of tropical central-eastern Pacific cooling for 1991–2014. Thus, the enhanced connection found between TRS summer precipitation and ENSO is partially attributed to enhanced latent heating of atmospheric moisture over the Maritime Continent, which is fundamentally attributable to increased atmospheric moisture content under global warming.

In addition, different SST anomalies are also observed for two periods of an El Niño-decaying summer (figure not shown). Positive (insignificant) SST anomalies are observed over the Arabian Sea during an El Niño-decaying summer of 1991–2014 (1961–1980). This difference also contributes to a different relationship between

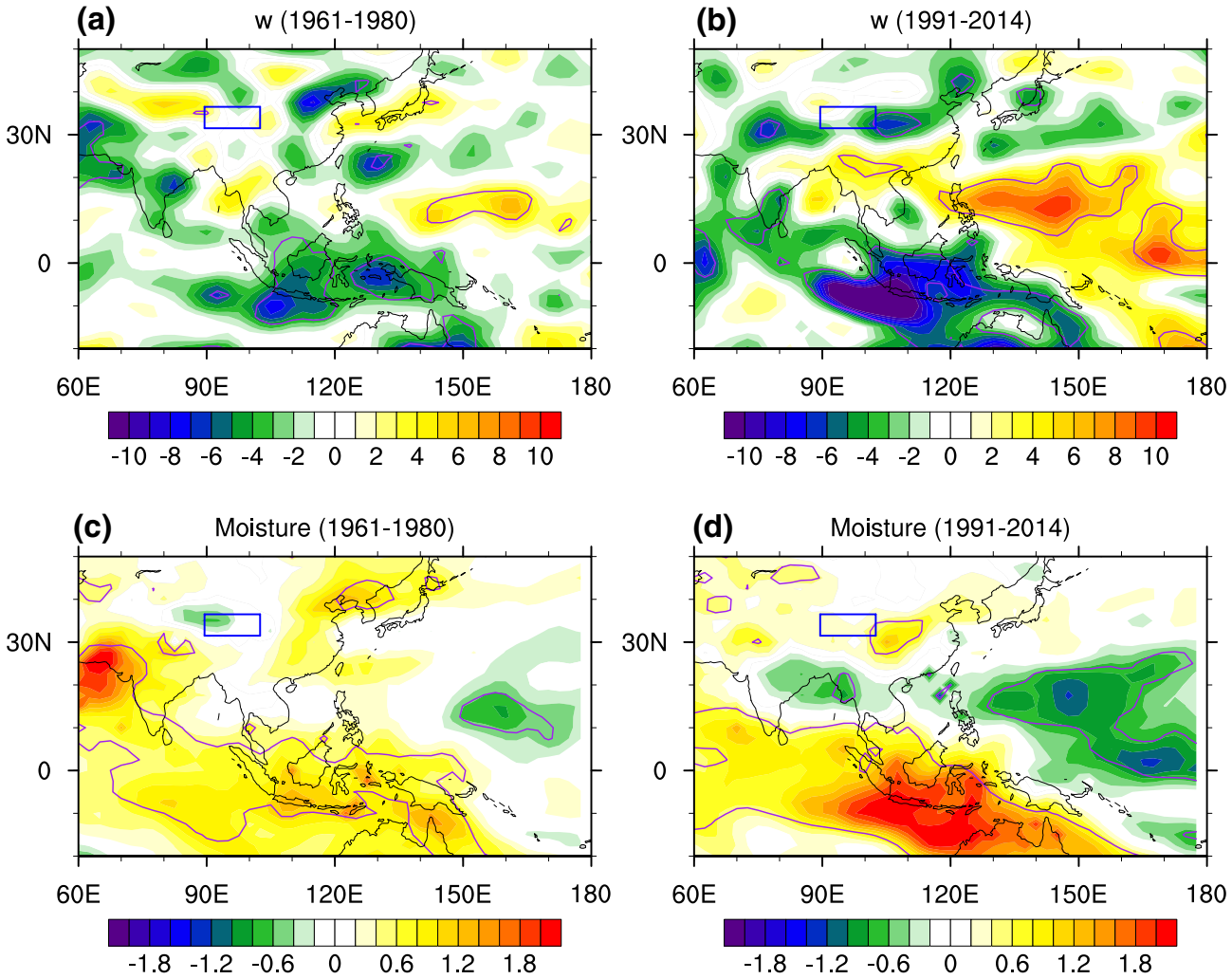

Fig. 11 Anomalies of **a, b** 500 hPa vertical velocity (unit: Pa s^{-1}) and **c, d** vertically integrated atmospheric moisture (unit: kg m^{-2}) regressed on the detrended and standardized time series of the sign-reversed Niño 3.4 tendency index for **a, c** 1961–1980 and **b, d** 1991–2014. Purple contours denote the 95% confidence level

TRS summer precipitation and preceding winter El Niño events for the two periods because of the effect of western Indian Ocean warming on TRS summer precipitation, as noted above.

The atmospheric circulation anomalies regressed on the sign-reversed Niño 3.4 index resemble atmospheric circulation anomalies regressed on the sign-reversed Niño 3.4 tendency index. In particular, significant negative anomalies of 500 hPa geopotential height found over the Indian Ocean correspond to a negative anomaly of the Niño 3.4 index for 1961–1980 and 1991–2014. These are not detected in atmospheric circulation anomalies corresponding to a negative anomaly of the Niño 3.4 tendency index. This discrepancy reveals different Indian Ocean summer climate during a summer of tropical central-eastern Pacific cooling and during an El Niño-decaying summer.

7 Enhanced connections to the EASM

Considering the significant correlation found between TRS summer precipitation and the EASM index for 9-year high-pass filtered time series of recent decades (Fig. 3d), the discussion presented in this section is mainly based on climate anomalies regressed on the 9-year high-pass filtered time series of the EASM index.

Figure 12 shows 500 hPa geopotential height anomalies and vertically integrated WVT anomalies associated with the EASM for 1961–1980 and 1991–2014. For 1961–1980, a strengthened EASM is mainly associated with an anomalous low over mid-latitudinal East Asia and with an anomalous high centered over the seas adjacent to eastern China (Fig. 12a). The anomalous low exerts northwesterly WVT anomalies over the TRS region, carrying cold and dry air into the TRS region and resulting in reduced atmospheric moisture over the TRS region. In contrast, from 1991 to

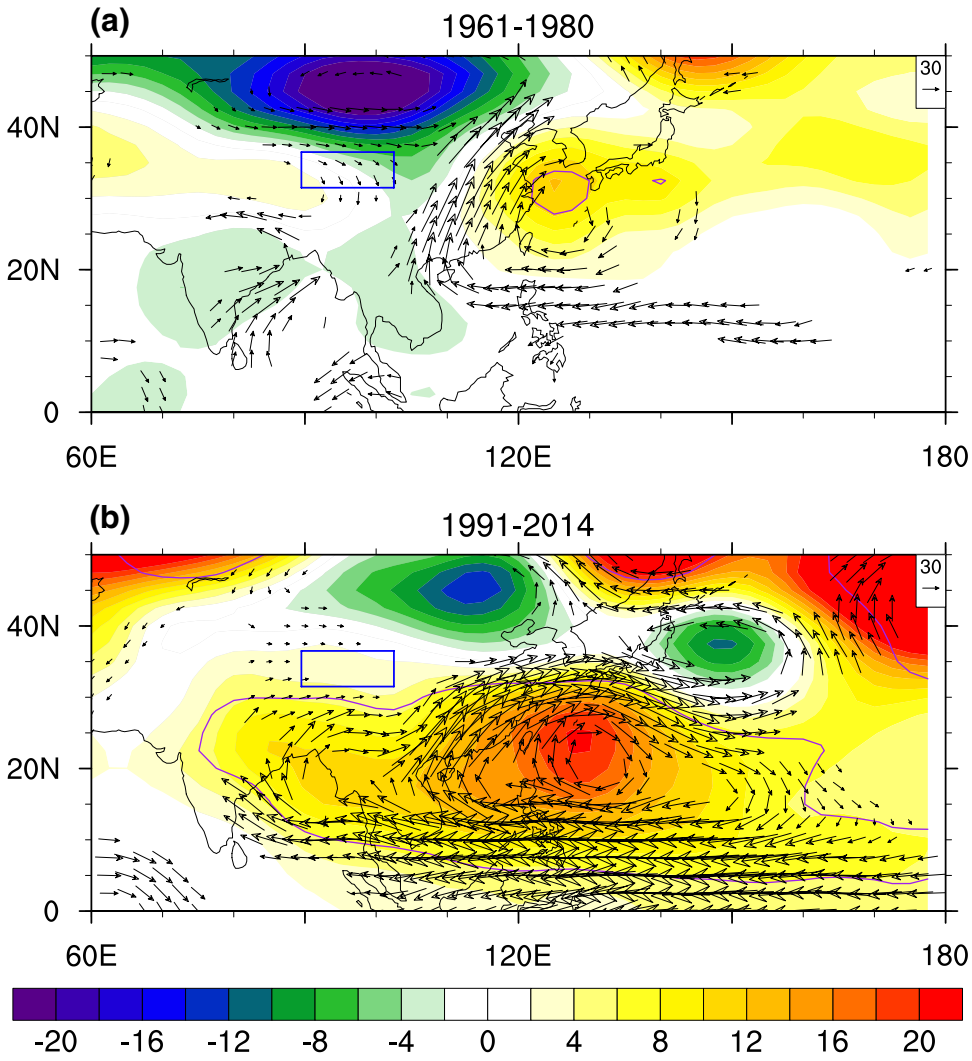

Fig. 12 Anomalies of 500 hPa geopotential height (colored shading, unit: gpm) and vertically integrated WVT (vectors, unit: kg m^{-1} s^{-1}) regressed on the standardized 9-year high-pass filtered time series for the EASM index for **a** 1961–1980 and **b** 1991–2014. Purple contours denote the 95% confidence level of 500 hPa geopotential height anomalies. Vectors are only shown for WVT anomalies significant at the 90% level

2014, a strengthened EASM is associated with a strong anomalous high extending from the WNP to the Bay of Bengal, inducing southwesterly WVT anomalies towards the TRS region that have important effects on TRS summer precipitation (Fig. 12b). Moreover, from 1991 to 2014, a strengthened EASM is associated with warming in the western Indian Ocean and in the tropical western Pacific whereas from 1961 to 1980, the EASM is associated with insignificant SST anomalies observed in the Indian Ocean and tropical western Pacific (Fig. 13). Thus, the enhanced connection found between TRS summer precipitation and the EASM may be essentially attributed to the enhanced impact of the Indian Ocean and ENSO on the anomalous high over the WNP and Bay of Bengal, as analyzed in Sects. 5 and 6.

The EASM is also associated with an Eurasian wave-train pattern observed in recent years, revealing an effect of climate signals from northern Europe and the North Atlantic on the EASM not observed for 1961–1980 (figure not shown). This Eurasian wave-train pattern somewhat resembles the Eurasian wave-train associated with summer NAO but with discernible differences. Further insight into this issue could facilitate a better understanding of EASM variability observed in recent years.

8 Conclusion and discussion

This study found an enhanced correlation between the interannual variability of TRS summer precipitation and NAO, AO, western Indian Ocean SST, ENSO, and the EASM, revealing an enhanced relationship between the summer climate over the TRS region and the global climate system. The comparison of associated climate anomalies for 1961–1980 and 1991–2014 shows that NAO has an enhanced influence on TRS summer climate via an anomalous Eurasian wave-train originating from the HB-DS region, which is stimulated by anomalous convective activity over the HB-DS region resulting from enhanced latent heating of atmospheric moisture. This enhanced effect of latent heating is also central to the enhanced influence of ENSO on TRS summer climate where convective activity over the Maritime Continent and associated PJ/EAP teleconnection pattern become more significant during an El Niño-decaying summer due to enhanced latent heating over the Maritime Continent observed in recent years, as well as during a summer of tropical central-eastern Pacific cooling. Western Indian Ocean warming has had a growing influence on TRS summer climate because of a shift in its warming center from south of the equator to north of the equator, which warrants further study.

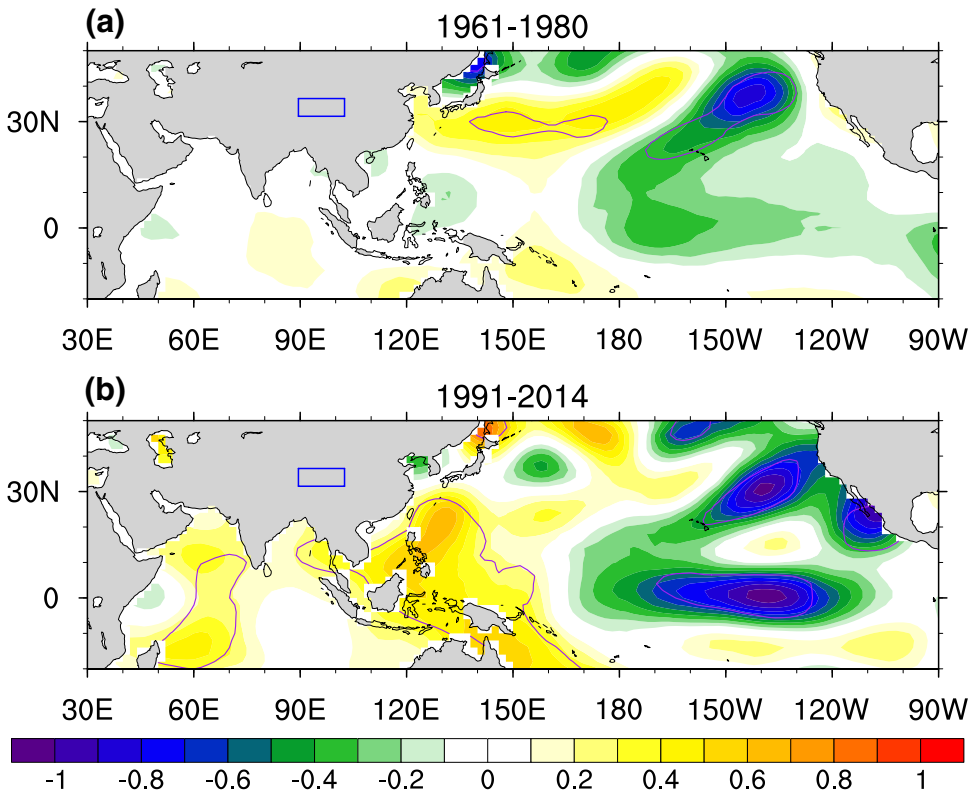

Fig. 13 Anomalies of SST (colored shading, unit: °C) regressed on the standardized 9-year high-pass filtered time series for the EASM index for **a** 1961–1980 and **b** 1991–2014. Purple contours denote the 95% confidence level

The enhanced connection found between TRS summer precipitation and the global climate system reflects the increasingly important effects of latent heating because of increased atmospheric moisture content around the globe under global warming. According to the Clausius–Clapeyron equation for saturation vapor pressure, water vapor increases by approximately 7% with 1 °C of warming (Held and Soden 2006). Correspondingly, a trend of increasing global atmospheric water vapor is found from observational and reanalysis data for the past several decades, although there are discrepancies between different datasets (Trenberth et al. 2005; Huntington 2006). Particularly for the Arctic region, a positive trend in column-integrated water vapor is observed for the northern North Atlantic that peaks during the summer (Serreze et al. 2012). These results and the results of this study highlight a need for more attention to the climate effects of increased atmospheric moisture content. In addition, the increased atmospheric moisture content observed over the Arctic is largely attributed to Arctic amplification, which is suggested to be essentially caused by diminishing sea ice (Screen and Simmonds 2010). Hence, the impacts of reduced Arctic sea ice on mid-latitudinal weather and climates also warrant examination with a focus on the role of increased atmospheric moisture (Liu et al. 2012; Li and Wang 2013, 2014).

The interannual variability of SST over the western Indian Ocean has undergone a shift in its warming center for unknown reasons. Hypothetically, this shift in the warming center over the western Indian Ocean may be related to a shift in the IOD mode inherent of the Indian Ocean (Saji et al. 1999). A series of questions can be raised on this issue. Is this shift in the warming center over the western Indian Ocean associated with ENSO? Is it mainly due to internal ocean variability or air–sea interactions (Hu and Li 2017)? How will it change in the future? All these questions require further study.

Although the correlation between the time series for TRS summer precipitation and the EASM index has been enhanced over past decades, an out-of-phase relationship between TRS summer precipitation and the EASM is observed in the time series after 2010. This implies the presence of uncertainty in the relationship between TRS summer precipitation and the EASM. The reason for this out-of-phase relationship after 2010 requires further study. In addition, other EASM indices should be used to examine the robustness of the results of this study.

Acknowledgements This study is funded by the National Key Research and Development Program of China (2016YFA0600703), the Jiangsu Innovation and Entrepreneurship Team, the Startup Foundation for Introducing Talent of NUIST (No. 2243141701093), and the Priority Academic Program Development of Jiangsu Higher Education Institutions (PAPD).

References

Chang CP, Zhang Y, Li T (2000) Interannual and interdecadal variations of the East Asian summer monsoon and tropical Pacific SSTs. Part I: roles of the subtropical ridge. J Clim 13:4310–4325

Chen W, Park JK, Dong B, Lu R, Jung WS (2012) The relationship between El Niño and the western North Pacific summer climate in a coupled GCM: role of the transition of El Niño decaying phases. J Geophys Res 117:D12111. https://doi.org/10.1029/2011JD017385

Chiang JCH, Swenson LM, Kong W (2017) Role of seasonal transitions and the westerlies in the interannual variability of the East Asian summer monsoon precipitation. Geophys Res Lett 44:3788–3795

Czaja A, Frankignoul C (2002) Observed impact of Atlantic SST anomalies on the North Atlantic Oscillation. J Clim 15:606–623

Duchon CE (1979) Lanczos filtering in one and two dimensions. J Appl Meteorol 18:1016–1022

Fan JW, Shao QQ, Liu JY, Wang JB, Harris W, Chen ZQ, Zhong HP, Xu XL, Liu RG (2010) Assessment of effects of climate change and grazing activity on grassland yield in the Three Rivers Headwaters region of Qinghai-Tibet Plateau, China. Environ Monit Assess 170:571–584

Francis JA, Vavrus SJ (2012) Evidence linking Arctic amplification to extreme weather in mid-latitudes. Geophys Res Lett 39:L06801. https://doi.org/10.1029/2012GL051000

Han T, He S, Hao X, Wang H (2017) Recent interdecadal shift in the relationship between Northeast China's winter precipitation and the North Atlantic and Indian Oceans. Clim Dyn. https://doi.org/10.1007/s00382-017-3694-x **(online pusblished)**

He S, Wang H (2013) Oscillating relationship between the East Asian winter monsoon and ENSO. J Clim 26:9819–9838

Held IM, Soden BJ (2006) Robust response of the hydrological cycle to global warming. J Clim 19:5686–5699

Hu WT, Li T (2017) Local intraseasonal air-sea relationship over the North Indian Ocean and western North Pacific during the spring-to-summer transition. Atmos Ocean Sci Lett 10:65–72

Huang RH (1992) The East Asia/Pacific pattern teleconnection of summer circulation and climate anomaly in East Asia. Acta Meteorol Sin 6:25–37

Huang BY et al (2015) Extended Reconstructed Sea Surface Temperature version 4 (ERSST. v4). Part I: upgrades and intercomparisons. J Clim 28:911–930. https://doi.org/10.1175/JCLI-D-14-00006.1

Huntington TG (2006) Evidence for intensification of the global water cycle: review and synthesis. J Hydrol 319:83–95

Hurrell JW, Kushinir Y, Ottersen G, Visbeck M (2003) An overview of the North Atlantic Oscillation. In: Hurrell JW, Kushnir Y, Ottersen G, Visbeck M (eds) The North Atlantic Oscillation: climatic significance and environmental impact. American Geophysical Union, Washington, pp 1–35. https://doi.org/10.1029/134GM01

Kalnay E, Kanamitsu M, Kistler R, Collins W, Deaven D, Gandin L, Iredell L, Saha S, White G, Woollen J, Zhu Y, Leetmaa A, Reynolds R, Chelliah M, Ebisuzaki W, Higgins W, Janowiak J, Mo KC, Ropelewski C, Wang J, Jenne R, Joseph D (1996) The NCEP/NCAR 40-year reanalysis project. Bull Am Meteor Soc 77:437–470

Li F, Wang H (2013) Autumn sea ice cover, winter Northern Hemisphere annular mode, and winter precipitation in Eurasia. J Clim 26:3968–3981

Li F, Wang H (2014) Autumn Eurasian snow depth, autumn Arctic sea ice cover and East Asian winter monsoon. Int J Climatol 34:3616–3625

Li S, Li D, Zhao P, Zhang G (2009) The climatic characteristics of vapor transportation in rainy season of the origin area of three

rivers in Qinghai-Xizang Plateau. Acta Meteorol Sin 67:591–598 **(in Chinese)**

Liu J, Curry JA, Wang H, Song M, Horton RM (2012) Impact of declining Arctic sea ice on winter snowfall. Proc Natl Acad Sci USA 109:4074–4079

Liu X, Zhang J, Zhu X, Pan Y, Liu Y, Zhang D, Lin Z (2014a) Spatiotemporal changes in vegetation coverage and its driving factors in the Three-River Headwaters region during 2000–2011. J Geogr Sci 24:288–302

Liu Y, Wang L, Zhou W, Chen W (2014b) Three Eurasian teleconnection patterns: spatial structures, temporal variability, and associated winter climate anomalies. Clim Dyn 42:2817–2839

Nitta T (1987) Convective activities in the tropical western Pacific and their impact on the Northern Hemisphere summer circulation. J Meteor Soc Jpn 65:373–390

Plumb RA (1985) On the three-dimensional propagation of stationary waves. J Atmos Sci 42:217–229

Qian S, Fu Y, Pan F (2010) Climate change tendency and grassland vegetation response during the growth season in Three-River Source region. Sci China Earth Sci 53:1506–1512. https://doi.org/10.1007/s11430-010-4064-2

Robertson AW, Mechoso CR, Kim YJ (2000) The influence of Atlantic sea surface temperature anomalies on the North Atlantic Oscillation. J Clim 13:122–138

Rodwell MJ, Rodwel DP, Folland CK (1999) Oceanic forcing of the wintertime North Atlantic Oscillation and European climate. Nature 398:320–323

Saji NH, Goswami BN, Vinayachandran PN, Yamagata T (1999) A dipole mode in the tropical Indian Ocean. Nature 401:360–363

Schott FA, Xie SP, McCreary JP Jr (2009) Indian Ocean circulation and climate variability. Rev Geophys 47:RG1002

Screen J, Simmonds I (2010) The central role of diminishing sea ice in recent Arctic temperature amplification. Nature 464:1334–1337

Serreze MC, Barrett AP, Stroeve J (2012) Recent changes in tropospheric water vapor over the Arctic as assessed from radiosondes and atmospheric reanalyses. J Geophys Res 117:D10104. https://doi.org/10.1029/2011JD017421

Song F, Zhou T (2014) The climatology and interannual variability of East Asian summer monsoon in CMIP5 coupled models: does air–sea coupling improve the simulations? J Clim 27:8761–8777

Sun J, Wang H (2012) Changes of the connection between the summer North Atlantic Oscillation and the East Asian summer rainfall. J Geophys Res 117:D08110. https://doi.org/10.1029/2012JD017482

Sun B, Wang H (2015) Inter-decadal transition of the leading mode of inter-annual variability of summer rainfall in East China and its associated atmospheric water vapor transport. Clim Dyn 44:2703–2722

Sun B, Wang H (2018) Interannual variation of the spring and summer precipitation over the Three-River-Source region in China and the associated regimes. J Clim. https://doi.org/10.1175/JCLI-D-17-0680.1

Sun B, Zhu Y, Wang H (2011) The recent interdecadal and interannual variation of water vapor transport over eastern China. Adv Atmos Sci 28:1039–1048

Trenberth KE, Fasullo J, Smith L (2005) Trends and variability in column-integrated atmospheric water vapor. Clim Dyn 24:741–758

Wang H (2002) The instability of the East Asian summer monsoon-ENSO relations. Adv Atmos Sci 19:1–11

Wang H, He S (2012) Weakening relationship between East Asian winter monsoon and ENSO after mid-1970s. Chin Sci Bull 57:3535–3540. https://doi.org/10.1007/s11434-012-5285-x

Wang B, Wu R, Fu X (2000) Pacific-East Asian teleconnection: how does ENSO affect East Asian climate? J Clim 13:1517–1536

Wu J, Gao XJ (2013) A gridded daily observation dataset over China region and comparison with the other datasets. Chin J Geophys 56:1102–1111. https://doi.org/10.6038/cjg20130406 **(in Chinese)**

Wu B, Zhou T, Li T (2009) Seasonally evolving dominant interannual variability modes of East Asian climate. J Clim 22:2992–3005

Xie SP, Hu K, Hafner J, Tokinaga H, Du Y, Huang G, Sampe T (2009) Indian Ocean capacitor effect on Indo-western Pacific climate during the summer following El Nino. J Clim 22:730–747

Xue F, Zhao JJ (2017) Intraseasonal variation of the East Asian summer monsoon in La Nina years. Atmos Ocean Sci Lett 10:156–161

Yang J, Liu Q, Xie S-P, Liu Z, Wu L (2007) Impact of the Indian Ocean SST basin mode on the Asian summer monsoon. Geophys Res Lett 34:L02708. https://doi.org/10.1029/2006GL028571